Effects of the ecto-ATPase apyrase on microglial ramification and surveillance reflect cell depolarization, not ATP depletion

Christian Madry[a,b,1], I. Lorena Arancibia-Cárcamo[a,2], Vasiliki Kyrargyri[a,2], Victor T. T. Chan[a], Nicola B. Hamilton[a,c,1], and David Attwell[a,1]

[a]Department of Neuroscience, Physiology and Pharmacology, University College London, London WC1E 6BT, United Kingdom; [b]Institute of Neurophysiology, Charité Universitätsmedizin, 10117 Berlin, Germany; and [c]Wolfson Centre for Age-Related Diseases, King's College London, London SE1 1UL, United Kingdom

Edited by Ardem Patapoutian, Scripps Research Institute, La Jolla, CA, and approved January 3, 2018 (received for review August 31, 2017)

Microglia, the brain's innate immune cells, have highly motile processes which constantly survey the brain to detect infection, remove dying cells, and prune synapses during brain development. ATP released by tissue damage is known to attract microglial processes, but it is controversial whether an ambient level of ATP is needed to promote constant microglial surveillance in the normal brain. Applying the ATPase apyrase, an enzyme which hydrolyzes ATP and ADP, reduces microglial process ramification and surveillance, suggesting that ambient ATP/ADP maintains microglial surveillance. However, attempting to raise the level of ATP/ADP by blocking the endogenous ecto-ATPase (termed NTPDase1/CD39), which also hydrolyzes ATP/ADP, does not affect the cells' ramification or surveillance, nor their membrane currents, which respond to even small rises of extracellular [ATP] or [ADP] with the activation of K^+ channels. This indicates a lack of detectable ambient ATP/ADP and ecto-ATPase activity, contradicting the results with apyrase. We resolve this contradiction by demonstrating that contamination of commercially available apyrase by a high K^+ concentration reduces ramification and surveillance by depolarizing microglia. Exposure to the same K^+ concentration (without apyrase added) reduced ramification and surveillance as with apyrase. Dialysis of apyrase to remove K^+ retained its ATP-hydrolyzing activity but abolished the microglial depolarization and decrease of ramification produced by the undialyzed enzyme. Thus, applying apyrase affects microglia by an action independent of ATP, and no ambient purinergic signaling is required to maintain microglial ramification and surveillance. These results also have implications for hundreds of prior studies that employed apyrase to hydrolyze ATP/ADP.

microglia | apyrase | ATP | potassium | depolarization

ATP-mediated signaling is present in many tissues, but is particularly important for microglia, the brain's innate immune cells (1). Microglia constantly survey the brain by extending and retracting their processes to sense their environment (2) but also, in the case of sudden brain damage, promptly send out processes to quickly target and enclose the site of injury (3). The latter response is mediated by ATP released from the damage site activating microglial $P2Y_{12}$ receptors (4, 5), but there is controversy over whether constant surveillance by microglia depends on activation of receptors by an ambient level of ATP or ADP in the extracellular solution. Understanding what drives surveillance is important because it enables microglia to detect brain damage or infection (6, 7) but also to monitor and modulate the functional state of synapses and neurons (8–10), remove excessively generated synapses by pruning them during brain development (11, 12), and regulate the number of neurons through phagocytic removal of surplus progenitor cells produced during development and adulthood (13, 14).

Several studies have reported that exposure to the ATP/ADP-hydrolyzing enzyme apyrase, both in vivo and in brain slices, evokes a rapid retraction of microglial processes and a reduction of surveillance (3, 15–17). This implies that a tonic extracellular purinergic signal may be needed to maintain microglial ramification and surveillance. Such a signal would imply a constant release of ATP into the extracellular space around microglial cells, and hydrolysis via ADP into AMP and adenosine by the activity of endogenous membrane-bound ecto-ATPases, such as the microglial-bound NTPDase1/CD39 (18) and the less selectively expressed 5′-nucleotidase CD73 (reviewed in ref. 19). Since a rise of extracellular [ATP] acts as a potent danger signal in the brain, triggering a rapid immunological response, these ecto-ATPases maintain a very low extracellular ATP concentration, in the low nanomolar range (20–23). This low concentration is expected to be insufficient to activate even those purinergic receptors which display the highest affinity, such as the microglial ADP-preferring $P2Y_{12}$ subtype with an EC_{50} of ∼100 to 200 nM (24). In agreement with this, recent reports show that microglial surveillance and ramification are independent of $P2Y_{12}$ receptor signaling (5, 25, 26), raising the question of how application of apyrase to lower extracellular nucleotide levels could affect microglial ramification and surveillance.

Apyrase, purified from potato or recombinant organisms (27), is an ecto-ATPase which hydrolyzes a wide range of nucleotide (N) substrates including ATP and ADP, according to the general reaction NTP → NDP + P_i → NMP + 2P_i. Ectopically applied

Significance

ATP mediates interactions between cells in many tissues, but is particularly important for microglia, the brain's immune cells, which constantly survey the brain to detect infection and regulate the brain's wiring during development. It is controversial whether the ceaseless movement of microglia is driven by ATP release from brain cells. We show that an enzyme (apyrase) widely used to manipulate ATP levels is contaminated with K^+ ions which inhibit microglial surveillance, and that no ATP release is needed to drive microglial process movement. Thus, all conclusions about a role of ATP in signaling based on applying apyrase need reexamining, and brain immune surveillance is not regulated by ATP release.

Author contributions: C.M. and D.A. conceived the paper; C.M., I.L.A.-C., V.K., V.T.T.C., and N.B.H. designed research; C.M., I.L.A.-C., V.K., V.T.T.C., and N.B.H. performed research; C.M., I.L.A.-C., V.K., V.T.T.C., and N.B.H. analyzed research; and C.M. and D.A. wrote the paper.

The authors declare no conflict of interest.

This article is a PNAS Direct Submission.

[1]To whom correspondence may be addressed. Email: christian.madry@charite.de, nicola.hamilton-whitaker@kcl.ac.uk, or d.attwell@ucl.ac.uk.

[2]I.L.A.-C. and V.K. contributed equally to this work.

This article contains supporting information online at www.pnas.org/lookup/suppl/doi:10.1073/pnas.1715354115/-/DCSupplemental.

apyrase is used widely to deplete endogenous nucleotides in biological preparations. Indeed, over 600 papers in PubMed report applying apyrase to perturb signaling mediated by extracellular ATP, on the assumption that this enzyme is acting by hydrolyzing ATP and other nucleotides.

By using a combination of pharmacology, electrophysiology, ion-sensitive electrode measurements, protein dialysis, and two-photon and confocal microscopy of microglial cells in acute hippocampal slices, we show that the apyrase-evoked reduction of microglial ramification and surveillance is not due to an abolition of tonic purinergic signaling. Instead, it is mediated by cell depolarization produced by the high $[K^+]$ content of commercially available apyrase. A similar depolarization produced by raising the extracellular $[K^+]$ ($[K^+]_e$) in the absence of apyrase has the same effects on ramification and surveillance, and dialyzing out the contaminating K^+ abolishes the effect of apyrase while retaining its enzymatic activity. These results have important implications for our understanding of what drives microglial surveillance, but also for all experiments investigating purinergic signaling that employ apyrase to lower ATP levels.

Results

Apyrase Decreases Microglial Ramification and Surveillance. To test for an effect of putative tonic ATP-mediated signaling on microglial morphology, we exposed acutely prepared postnatal day (P)12 rat hippocampal slices to the ATP-hydrolyzing enzyme apyrase (200 U/mL, Sigma A7646, was used for all experiments except where indicated otherwise) for 30 min. After fixation of the tissue and immunolabeling microglia for Iba-1, we quantified their process ramification by performing a three-dimensional Sholl analysis. Individual microglial cells were analyzed at a depth of at least 60 μm below the slice surface (to avoid any effects due to slicing-evoked superficial cell damage) in high-resolution confocal image stacks. While untreated microglial cells (control) displayed a ramified morphology with a large number of long and highly branched processes (Fig. 1*A*), microglia exposed to apyrase had much shorter and less complex processes, covering a markedly reduced area compared to their untreated counterparts (Fig. 1*B*). The Sholl analysis showed that apyrase treatment reduced the number of intersections of microglial processes with concentric Sholl spheres at increasing distances from the soma (Fig. 1*C*), and reduced the number of branch points and process terminals (Fig. 1 *D* and *E*).

To investigate how microglial surveillance is affected by apyrase exposure in real time, we imaged microglia in hippocampal slices using two-photon microscopy and quantified changes of baseline surveillance and ramification minute by minute (*Materials and Methods*). Apyrase was locally applied to individual microglial cells through a pipette inserted into the tissue ~10 to 20 μm away from the cell's soma. This caused a rapid retraction of microglial processes (Fig. 1*F*) and decreased both the surveillance and ramification indices in a dose-dependent manner (Fig. 1 *G–J*), whereas performing the same manipulation with extracellular solution in the pipette (Fig. 1 *G* and *H*) had no effect (to allow local application of apyrase to raise its concentration around the cell significantly in this experiment, the rate of superfusion of extracellular solution was low, which is why the apyrase-evoked change does not reverse rapidly under these live imaging conditions, but recovery was seen using a different approach in Fig. 3*M* below). Thus, apyrase induces a strong and rapid loss of microglial processes, which would conventionally be interpreted as indicating the existence of a tonic extracellular purinergic signal maintaining microglial ramification and surveillance.

To test this hypothesis, we next assessed whether there is a detectable ATP concentration in the extracellular space of brain tissue, using ATP-evoked chemiluminescence of firefly luciferase enzyme. This emits photons that can be detected with a photomultiplier tube (PMT), with a quantum yield of almost one photon per ATP molecule and a detection limit of <1 nM ATP (28, 29). Brief puffs (0.5 s) of 1 mM ATP in extracellular solution produced a robust PMT-mediated current, which was greatly reduced in the presence of 100 U/mL apyrase (Fig. 1 *K* and *L*), showing that added apyrase effectively hydrolyzes extracellular ATP. However, when imaging the ATP-evoked signal from a hippocampal slice without any puffed ATP, we could not detect any difference in signal amplitude if the slice was removed (Fig. 1*L*, *Inset*), implying (surprisingly, given the effect of apyrase described above) that the extracellular ATP concentration in slices is kept at a very low level, below the detection limit of this assay.

Lack of a Tonic ATP Release Mechanism in Baseline Conditions. To further test whether extracellular ATP may be required to keep microglia motile and ramified, we next performed experiments interfering with ATP metabolism in brain tissue. Microglia express on their surface membrane high amounts of the ecto-ATPase NTPDase1/CD39 (18), which hydrolyzes ATP or ADP into AMP which, in turn, is hydrolyzed into adenosine by other types of ecto-enzyme (for a review, see ref. 30). This entire ecto-nucleotidase pathway operates very rapidly, with a half-time for the conversion of ATP to adenosine of only ~200 ms (31). Thus, if there is an ambient level of ATP present around microglial cells then there needs to be a tonic release of ATP which will be constantly hydrolyzed into ATP breakdown products. Consequently, blockade of ecto-ATPases should lead to an accumulation of extracellular ATP in slices (32). Microglia are very sensitive to increases of extracellular ATP concentration, to which they respond by activating $P2Y_{12}$ receptor-gated THIK-1 K^+ channels, generating an outward K^+ current which leads to a hyperpolarization of their membrane (33). Puff application of ATP (or ADP) to the slice surface caused a dose-dependent activation of this outward K^+ current in whole-cell voltage-clamped microglia held at 0 mV (Fig. 2*A*), which evoked a hyperpolarization in unclamped cells (Fig. 2*A*, *Inset*). Notably, even concentrations of ATP as low as 100 nM generated a clearly visible electrical response, emphasizing that microglial cells can sense even a subtle rise of extracellular ATP concentration due to their expression of high-affinity $P2Y_{12}$ receptors (5, 24).

Despite their sensitivity to ATP, the microglial resting membrane potential (Fig. 2 *B* and *C*) and current (Fig. 2*D*, red dashed line) were not detectably affected by the application of 200 μM ARL-67156 (Fig. 2 *B–D*), a widely used broad-spectrum NTPDase blocker (34, 35). Confirming that it did block endogenous ecto-ATPases, however, ARL-67156 evoked a robust ~60% increase of the K^+ current evoked by brief puffs of ATP (Fig. 2 *D* and *E*). This demonstrates that ARL-67156 effectively blocks the hydrolysis of exogenously applied ATP, thus potentiating its action, whereas no detectable turnover of ATP occurs in baseline conditions (Fig. 2 *B* and *C*), suggesting that endogenous ATP levels are very low.

Any rise of extracellular ATP which might occur following ecto-ATPase block is also expected to induce changes of microglial surveillance and ramification (16, 36). To try to detect this, we imaged microglial motility by two-photon microscopy as in Fig. 1. Microglial cells were imaged at least 60 μm below the slice surface and exhibited a ramified morphology with highly motile processes showing constant extensions and retractions over time (Fig. 2*F*). After an initial 20-min control period, we blocked ecto-ATPases by bath applying 200 μM ARL-67156. However, neither microglial surveillance nor ramification (Fig. 2 *G–J*) was affected, again suggesting that the extracellular ATP concentration remained unaltered, and hence that little ATP is being released in the slice (in the absence of tissue damage).

In summary, chemiluminescence, electrophysiology, and imaging experiments exclude the existence of a baseline extracellular ATP concentration high enough to drive microglial purinergic signaling.

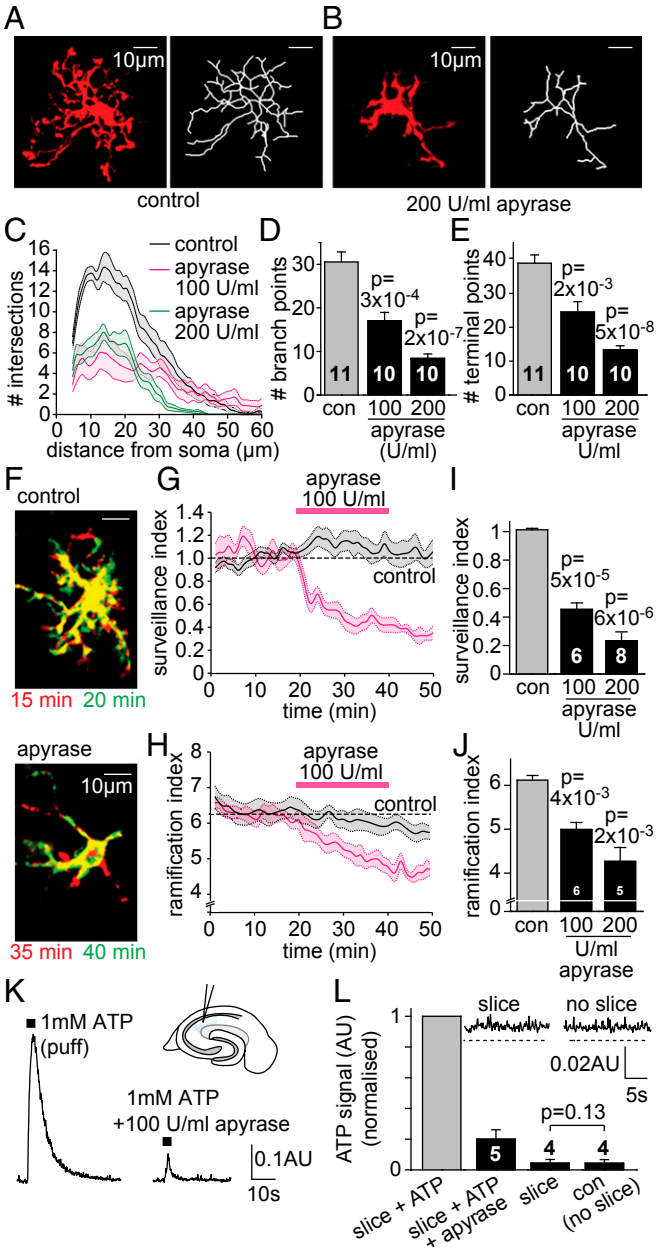

Fig. 1. Apyrase reduces microglial ramification and surveillance. (*A* and *B*) Specimen images (*Left*) and skeletonized arbors (*Right*) of rat hippocampal microglia labeled with antibody to Iba-1 after superfusion with (*A*) control solution and (*B*) solution containing 200 U/mL apyrase (Sigma; A7646). (*C–E*) Three-dimensional Sholl analysis-derived values of the number of process intersections with spherical shells at different distances from the soma (*C*; control and 200 U/mL curves differ significantly, $P = 0.0058$), number of cell branch points (*D*), and number of process ends (*E*) for microglia in control solution or solution containing 100 or 200 U/mL apyrase. Numbers of cells are on bars. (*F–J*) Effect of apyrase on microglial surveillance and ramification. (*F*) Color-coded superimposed images at 15 and 20 min in control solution (*Top*) and at 35 and 40 min after starting apyrase superfusion at *t* 20 min (*Bottom*; green, process extensions; red, process retractions; yellow, no change). (*G* and *H*) Plots of surveillance index (*G*) and ramification index (*H*) against time when individual microglia are exposed to apyrase (via a puffing pipette inserted into the slice). Control data (gray) show experiments with the puffing pipette filled with extracellular solution. (*I* and *J*) Surveillance index (*I*; *Materials and Methods*) and ramification index (*J*) in control solution and 100 and 200 U/mL apyrase. (*K*) Luciferin-luciferase luminescence (PMT current; AU, arbitrary units) evoked by ATP puff in control solution and solution containing apyrase (without a slice) illustrating that apyrase effectively degrades the puffed ATP (*Inset* schematic shows the experimental setup, with blue showing the hippocampal stratum radiatum). (*L*) Mean luciferin-luciferase signal evoked by puffing 1 mM ATP onto a slice in the absence and presence of 100 U/mL apyrase (as in *K*), generated by a slice with no puffed ATP, and the baseline signal generated in the absence of a slice (con). (*L*, *Inset*) Records for the last two conditions with dashed lines showing no signal. Data are presented as mean ± SEM.

Thus, the apyrase-evoked decrease of microglial surveillance and ramification is unlikely to reflect hydrolysis of extracellular ATP.

Apyrase Depolarizes Microglia Due to Its High K^+ Content. We have recently shown that microglial surveillance and ramification are regulated by the cell's resting membrane voltage, which is set by the tonic activity of its K^+ channels, such that pharmacological block or knockout of the main microglial K^+ channel (THIK-1) evokes depolarization of the cell and a loss of ramification and surveillance (33). Surprisingly, application of apyrase to hippocampal slices evoked a strong and reversible dose-dependent depolarization of current-clamped microglial cells (Fig. 3 *A* and *B*). In some experiments, to prevent any putative purinergic signaling between microglia and their surrounding cells, we carefully lifted the whole-cell patch-clamped cell out of the slice while maintaining the whole-cell configuration (Fig. 3*C*). After isolating the cell from its native environment, we confirmed that it still responded to brief puffs of ATP by generating outward K^+ currents (Fig. 3*C*). Exposure to apyrase evoked an inward membrane current at a holding potential of 0 mV (Fig. 3*C*, arrow), which we will show below results from a rise in $[K^+]_e$ decreasing K^+ efflux occurring at 0 mV through tonically active potassium channels. Apyrase also diminished the ATP-evoked outward K^+ current, which could reflect both a decrease in the driving force for K^+ efflux and apyrase hydrolyzing some of the puff-applied ATP (Fig. 3*C*). A detailed analysis of the effects apyrase has on the electrophysiology of microglia is given in *Supporting Information* (see also Fig. S1).

To test the idea that apyrase raises the extracellular $[K^+]$, we measured $[K^+]_e$ using K^+-sensitive electrodes inserted into the slice. Indeed, application of apyrase to slices led to a dramatic rise of $[K^+]_e$ (Fig. 3*D*), which was dose-dependent and did not require a slice to be present at all (Fig. 3*E*). Thus, the apyrase solution contained, apart from the actual enzyme, also high amounts of potassium. The apyrase that we tested in most of our experiments is a very commonly used type (catalog no. A7646) from Sigma, the largest supplier with the greatest varieties of different apyrase preparations extracted either from potato (the majority) or recombinantly expressed. A literature search revealed that the vast majority of researchers obtained apyrase from Sigma, most commonly the preparations A6132, A6410, A6535, and A7646, which vary in the apyrase units per mg protein and purification grades. We therefore compared the resulting potassium concentrations of six different and frequently used apyrase preparations made up at 100 U/mL each (in standard extracellular solution containing 2.5 mM $[K^+]$ in the absence of apyrase; *Materials and Methods*) using a commercial blood-gas analyzer. All preparations had significantly elevated $[K^+]$ contents, which correlated roughly inversely with the number of units of enzyme per mg of solid preparation (Fig. 3 *F* and *G*). In the case of two apyrase types (A6132 and A6237), $[K^+]_e$ reached extremely high concentrations in the range of 30 to 40 mM $[K^+]$, even at 100 U/mL, a concentration frequently used in published experiments in tissue slices or in vivo (100 to 500 U/mL).

Next, we tested the effect of an elevated potassium concentration (raised by 20 mM, to a total of 22.5 mM, with $[Na^+]$ lowered correspondingly) on microglial morphology in the absence of any apyrase, using Sholl analysis as in Fig. 1. A 30-min exposure of slices to 22.5 mM $[K^+]$, which roughly equates to the $[K^+]$ present in the slices in 200 U/mL apyrase (A7646) (Fig. 3 *D*

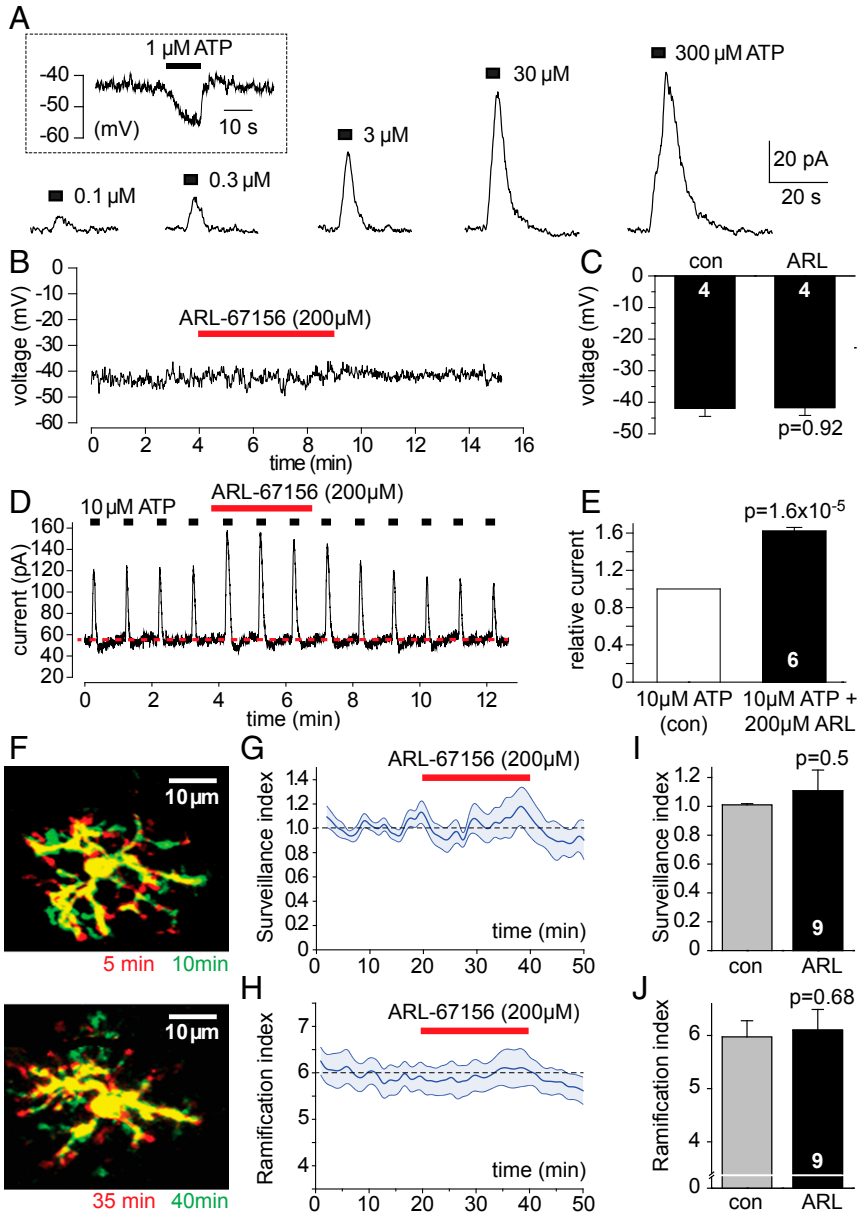

Fig. 2. Tonic ATP release does not maintain microglial surveillance and ramification. (*A*) Current response of a microglial cell clamped to 0 mV to puffed ATP (black boxes). (*A*, *Inset*) Membrane potential response in an unclamped cell. (*B* and *C*) Inhibition of ecto-ATPases with ARL-67156 has no effect on microglial membrane potential (*B*, specimen trace; *C*, mean data; numbers of cells are on bars). (*D*) Ecto-ATPase inhibition potentiates current response at 0 mV to puffed ATP (black squares), but does not alter baseline current (red dashed line). (*E*) Mean normalized data for current evoked by puffed ATP in experiments like *D*, in the absence and presence of ARL-67156. (*F–J*) Effect of ecto-ATPase inhibition on microglial surveillance and ramification. (*F*) Color-coded superimposed images (as in Fig. 1*F*) at 5 and 10 min in control solution (*Top*) and at 35 and 40 min (*Bottom*) after starting ARL-67156 superfusion at *t* 20 min. (*G* and *H*) Time course of surveillance index (*G*) and ramification index (*H*) before and during superfusion of ARL-67156. (*I* and *J*) Mean normalized surveillance index (*I*) and ramification index (*J*) during superfusion of ARL-67156. Data are presented as mean ± SEM.

and *E*), caused a severe deramification of microglial cells (Fig. 3 *H–J*) with a strong reduction in the number of branch points and terminal processes (Fig. 3 *K* and *L*). The morphology in high $[K^+]_e$ almost exactly matched that seen with apyrase treatment as shown in Fig. 1, and led to a reduced rate of surveillance of the brain because of the smaller number of processes. The time course of the onset of the deramification, and of the recovery when apyrase or elevated $[K^+]_e$ was removed, was not significantly different (Fig. 3*M*; two-way ANOVA, $P = 0.68$). Thus, apyrase induces morphological changes in microglia by virtue of the high $[K^+]_e$ it contains, and not via ATP depletion.

Dialyzing Apyrase Retains Enzyme Activity but Abolishes Effects on Microglial Ramification and Hence Surveillance. To test whether there is any tonic purinergic signaling affecting microglial properties, which may have been masked by the high $[K^+]$ content present in the apyrase preparations, we removed the high $[K^+]$ by dialysis against normal extracellular solution. Using a dialysis membrane with a molecular weight cutoff (MWCO) of 2 kDa, salts and other small molecules below this threshold were removed while apyrase with a molecular weight of ∼45 kDa was retained.

We first verified that the dialyzed apyrase depleted [ATP] as effectively as the nondialyzed apyrase from the same batch by

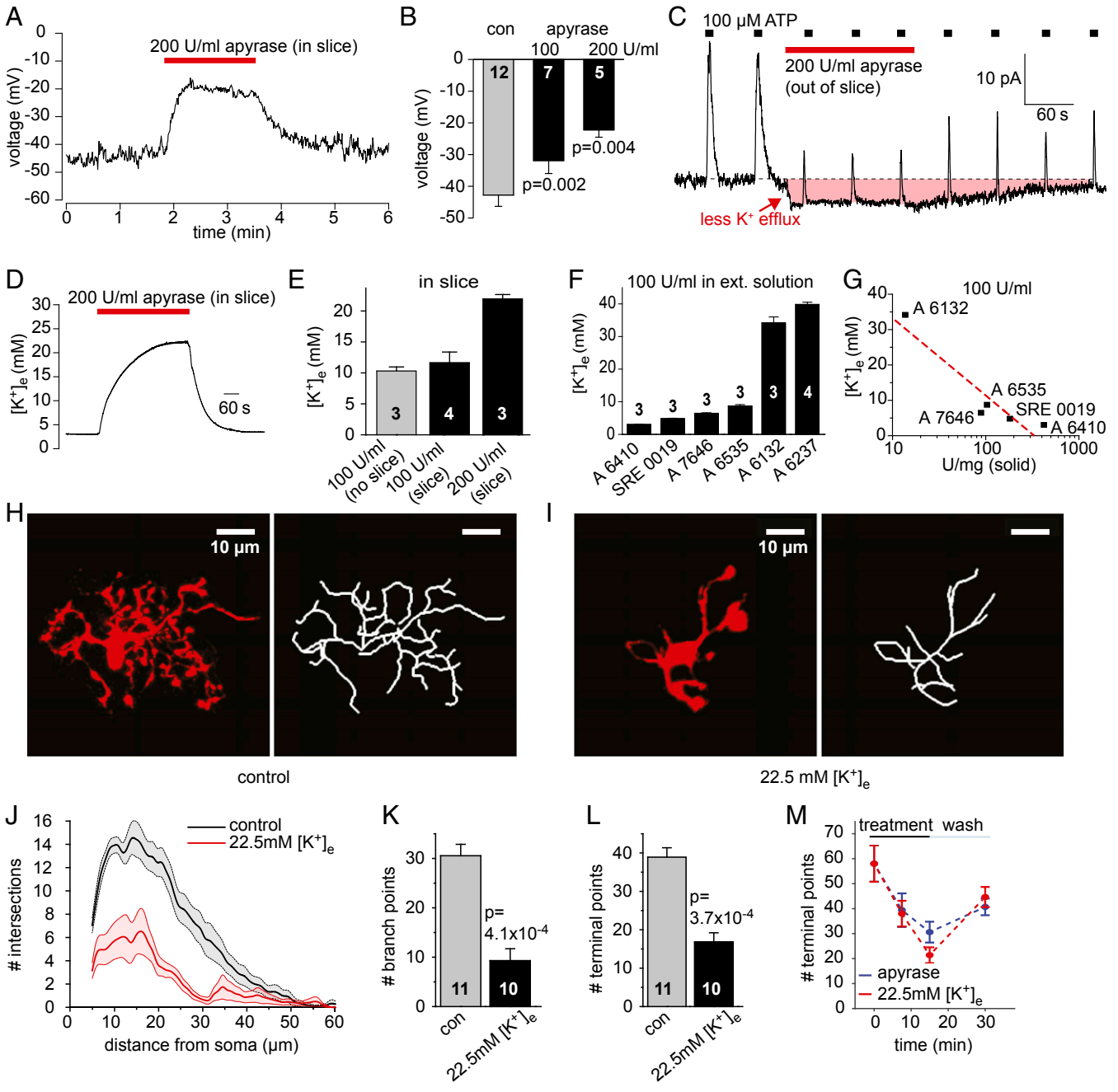

Fig. 3. Apyrase depolarizes microglia due to K^+ contamination. (*A*) Microglial membrane potential depolarization during superfusion of apyrase. (*B*) Mean membrane potential for microglia in control solution and in solution with 100 or 200 U/mL apyrase (Sigma; A7646) added. Numbers of cells are on bars; *P* values from *t* tests are for comparison with control solution. (*C*) Effect of apyrase (Sigma; A7646) on baseline membrane current at 0 mV of a microglial cell pulled out of the slice (apyrase evokes an inward current, shaded red) and on the response to puffed ATP (black squares, upward current deflections). (*D*) Specimen trace for measuring $[K^+]_e$ with a K^+-sensitive electrode in a slice during application of apyrase (Sigma; A7646). (*E*) Mean $[K^+]_e$ measurements (as in *D*) when applying 100 U/mL apyrase (Sigma; A7646) with no slice present or in a slice, or applying 200 U/mL apyrase to a slice. (*F*) $[K^+]_e$ measured with a blood-gas analyzer in extracellular solution to which different apyrase preparations were added at 100 U/mL (abscissa shows Sigma-Aldrich catalog numbers); values include the 2.5 mM K^+ in the extracellular solution recipe. (*G*) Plot of $[K^+]_e$ (ordinate) in extracellular solution containing 100 U/mL apyrase made up from sources of different purity (abscissa). (*H* and *I*) Specimen images (*Left*) and skeletonized arbors (*Right*) of rat hippocampal slice microglia labeled with antibody to Iba-1 after incubation with (*H*) control solution and (*I*) solution containing 22.5 mM K^+ for 30 min (see *Materials and Methods* for details). (*J–L*) Sholl analysis-derived values of the number of process intersections with spherical shells at different distances from the soma (*J*; control and 22.5 mM $[K^+]_e$ curves differ significantly, $P = 2.4 \times 10^{-4}$), number of cell branch points (*K*), and number of process ends (*L*) for slices exposed to control solution or solution containing 22.5 mM $[K^+]_e$ (numbers of cells are on bars). (*M*) Sholl analysis-derived numbers of process ends (reflecting microglial ramification) after different times of exposure to 22.5 mM $[K^+]_e$ or 200 U/mL apyrase, and after a 15-min washout, show a similar magnitude and time course of deramification and recovery for both conditions ($P = 0.68$, two-way ANOVA). Data are presented as mean ± SEM.

measuring chemiluminescence-derived signals as in Fig. 1*K*. As with the nondialyzed enzyme, dialyzed apyrase greatly reduced the luciferase signal evoked by an ATP puff (Fig. 4*A*), showing that dialysis did not affect the enzymatic activity of the apyrase.

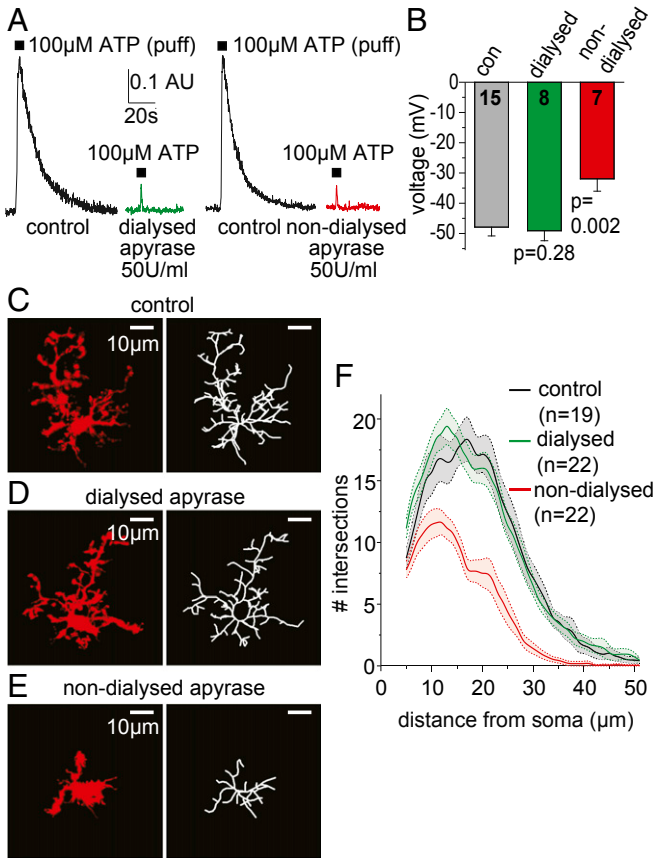

Fig. 4. Dialyzing apyrase retains microglial membrane potential and morphology. (*A*) The luciferin-luciferase PMT signal evoked by puffing ATP in extracellular solution (without a slice) is reduced by the same amount by dialyzed and undialyzed apyrase. (*B*) Resting potential of microglia in normal extracellular solution (con), solution with 100 U/mL dialyzed apyrase added (Sigma; A7646), and solution with 100 U/mL undialyzed apyrase added (as in Fig. 3*B*). Numbers of cells are on bars. (*C–E*) Specimen images (*Left*) and skeletonized arbors (*Right*) of rat hippocampal slice microglia labeled with antibody to Iba-1 after incubation with (*C*) control solution, (*D*) solution containing dialyzed apyrase (200 U/mL apyrase; Sigma; A7646), and (*E*) solution containing nondialyzed apyrase. (*F*) Three-dimensional Sholl analysis-derived values of the number of process intersections with spherical shells at different distances from the soma for microglia superfused with the solutions in *C–E*. Control and nondialyzed apyrase curves differ significantly, $P = 2.9 \times 10^{-3}$, whereas no difference exists between control and dialyzed apyrase, $P = 0.91$. Data are presented as mean ± SEM.

However, 200 U/mL dialyzed apyrase had no effect on the resting membrane potential (Fig. 4*B*) and did not alter the membrane current of the microglia (Fig. S2), while the same batch of nondialyzed apyrase depolarized the cells (Fig. 4*B*), evoked an inward membrane current at 0 mV, and increased the cells' conductance at negative potentials (see Fig. S2 and *Supporting Information* for detailed analysis). This clearly demonstrates that $[K^+]$ has been effectively removed from the apyrase preparation and furthermore indicates that no tonic ATP levels are present and necessary to maintain the resting potential of microglial cells.

Finally, we investigated the effect of dialyzed apyrase, which should lower the extracellular ATP concentration without raising $[K^+]_e$, on microglial morphology, using Sholl analysis. Strikingly, microglial cells remained as ramified as under untreated control conditions when exposed to 200 U/mL dialyzed apyrase (Fig. 4 *C*, *D*, and *F*), while 200 U/mL of the nondialyzed enzyme induced the expected decrease in process ramification (Fig. 4 *E* and *F*). Thus, all of the effects of undialyzed apyrase on microglial ramification, and hence on surveillance, which is reduced when there are fewer processes, are produced by the high $[K^+]$ present in this product and not by ATP depletion.

Discussion

Microglial ramification and process movement are critical for normal brain function, since they underpin the ability of these cells to constantly survey the brain. This surveillance is thought to allow the cells not only to detect invading microorganisms but also to prune redundant synapses during development and regulate neuronal activity. It has been suggested that microglial surveillance may require tonic ATP-evoked signaling in microglia, in part on the basis of experiments lowering the extracellular ATP concentration by applying the ATPase apyrase, which we now show is contaminated by K^+ ions which will depolarize the microglia. Using dialyzed, purified apyrase allowed us to investigate the role of endogenous nucleotides in regulating microglial surveillance and morphology, without a superimposed elevation of external $[K^+]$ which may generate effects independent of purinergic signaling.

Our findings show that microglial cells do not receive any tonic purinergic input that is required to maintain their morphology and constant surveillance in the healthy brain. Surprisingly, the reduced ramification and surveillance evoked by apyrase that we and others have observed are not due to its enzymatic activity but are produced by the high $[K^+]$ content present in commercially available apyrase preparations, which causes a significant depolarization of the cells. We have recently shown that such a depolarization is sufficient to dramatically reduce microglial ramification and surveillance, which are regulated and maintained by the cell's resting potential, which is set by the tonic activity of the cells' K^+ channels (33). Fig. 3 *H–M* shows the direct effect of depolarization by high $[K^+]_e$ on hippocampal microglial morphology [since microglia may vary in their properties according to brain region (37), the magnitude of the effect of depolarization on microglial morphology may vary between brain regions]. The rise of $[K^+]_e$ to ∼60 mM that occurs during the spreading depression associated with migraine, stroke, subarachnoid hemorrhage, or brain injury (38), or the anoxic depolarization induced by ischemia (39), and the 10 mM $[K^+]_e$ rise occurring during synchronous high-frequency activity of neurons in epilepsy (39) are expected to depolarize microglia and decrease their ramification and surveillance. In contrast, the $[K^+]_e$ rise occurring during normal neuronal activity [∼1 mM (39)] is much smaller and will have little effect.

Nonactivated microglial cells selectively express G_i protein-coupled $P2Y_{12}$ receptors (5, 40), which exhibit a very high affinity for adenosine nucleotides, with an EC_{50} value for ADP in the range of ∼100 nM (24). In addition, these receptors are linked to the activation of microglial K^+ channels (33), hence making the $P2Y_{12}$–K^+ channel signaling complex an ideal sensor to translate even subtle rises of ATP or ADP concentration into an electrical signal or other downstream messengers. It was not surprising, then, that several studies reported that microglial morphology and surveillance are regulated by a tonic purinergic input that is essential for keeping the cells ramified and motile. These conclusions were obtained (Fig. 5) by applying exogenous apyrase (3, 15–17), or knocking out the endogenous ecto-ATPase (NTPDase1/CD39) (18, 41), to manipulate the extracellular nucleotide levels produced by any tonic nucleotide release that does occur. However, our results show that nonactivated microglia receive no tonic purinergic input to maintain their ramification and surveillance, since application of dialyzed, $[K^+]$-free apyrase evoked neither a change of their membrane currents nor of their morphology, indicating a lack of a tonic activation of microglial purinergic receptors. Consistent with our results, experiments with $P2Y_{12}$ receptors blocked or knocked

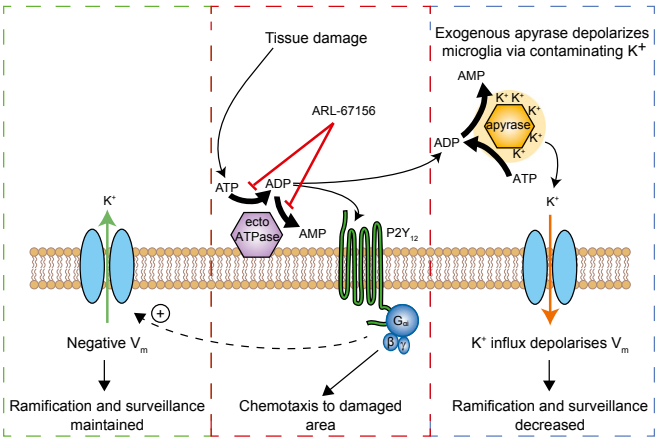

Fig. 5. Regulation of adenine nucleotide levels and microglial membrane potential. (*Left*; green box) Tonic activity of K^+ channels generates a K^+ efflux (green arrow) which maintains the resting potential of microglia, which is essential for the normal ramification of microglia and hence their normal level of surveillance. (*Middle*; red box) Tissue damage releases ATP. Endogenous ecto-ATPases on microglia and other brain cells hydrolyze ATP to ADP, and ADP to AMP (diagram shows ecto-ATPase only on microglia for simplicity). ADP, and possibly ATP, can activate $P2Y_{12}$ receptors on microglia. In the case of tissue damage, this evokes process outgrowth (chemotaxis) to the damaged area. $P2Y_{12}$ activation also increases the activity of microglial K^+ channels (Fig. 2*A*), allowing $P2Y_{12}$ receptors to be used to sense the baseline level of ATP/ADP (as in Fig. 2). If there is tonic ATP release in physiological conditions, blocking ecto-ATPases with ARL-67156 will elevate extracellular [ATP] and [ADP] and generate a membrane current. Fig. 2*D* (baseline current) shows that no such current is generated, implying that there is no detectable tonic activation of $P2Y_{12}$ receptors. (*Right*; blue box) Adding exogenous apyrase contaminated with K^+ raises $[K^+]_e$ artifactually and thus decreases the outward current through K^+ channels (shown as an inward shift of current; orange arrow), depolarizing the microglia and decreasing ramification and surveillance. Adding apyrase (dialyzed or undialyzed) will also lower the extracellular level of ATP and ADP, as demonstrated in Figs. 1*K* and 4*A*.

out, which abolished microglial process outgrowth in response to a sudden rise of $[ATP]_e$, had no effect on microglial surveillance, ramification, or membrane potential (5, 25, 26, 33).

Since a rise of extracellular nucleotides is recognized as a potent danger signal by microglia, tonic levels of ATP or ADP are normally kept very low (20–23, 42, 43), and our data suggest that they are not sufficient to tonically activate $P2Y_{12}$ receptors. Only when extracellular [ATP] and [ADP] rise significantly, for example due to brain damage, are $P2Y_{12}$ receptors effectively activated, to mediate rapid process extension to the site of injury (ATP leakage). This targeted motility depends on ecto-ATPases, since their inhibition with ARL-67156 abolishes the outgrowth of microglial processes to an ATP source (36, 44). This may involve the generation of ADP from ATP, to activate $P2Y_{12}$ receptors, but could also involve ecto-ATPase–mediated generation of adenosine which acts on microglial A_3-type adenosine receptors (41, 44, 45). Thus, ecto-ATPase regulation of extracellular nucleotide levels is important for targeted microglial motility evoked by a rise of extracellular ATP levels, but whether ecto-ATPases also contribute to microglial physiology in resting conditions, in the absence of any brain damage-derived ATP release, is more controversial.

Our results show that blocking ecto-ATPases (with ARL-67156) in resting conditions caused no changes of microglial ramification and surveillance, and did not evoke a $P2Y_{12}$ receptor-evoked electrical response in patch-clamped microglial cells. In contrast to our finding, Matyash et al. (41) have found that microglial cells were less ramified when NTPDase1 (CD39) is knocked out, suggesting that constitutive ATP/ADP breakdown by NTPDase1 and tonic activity of $P2Y_{12}$ and adenosine receptors are required to maintain a ramified microglial morphology. However, in these studies, NTPDase1 was globally knocked-out and the effects on microglial morphology of a direct, pharmacological inhibition or microglial-specific knockout were not tested. This is important, since NTPDase1-mediated effects can also originate from other cells (46). NTPDase1 is also prominently expressed at the surface of vascular smooth muscle cells (18, 40), where it contributes to the regulation of vascular tone and modulates vascular inflammation and thrombosis (47–49). Since microglial cells are in constant, bidirectional communication with blood vessels and endothelial cells (50, 51), the less ramified morphology observed in NTPDase1 KO animals may be the result of a primed or chronically activated phenotype originating from an altered microenvironment around blood vessels. Furthermore, NTPDase1 exhibits functions beyond its enzymatic activity by interacting with Ran binding protein M (RanBPM) through its cytoplasmic N-terminal domain (52). RanBPM is ubiquitously expressed in the brain and acts as an intracellular signaling hub for a variety of signaling proteins including surface β-integrins (53), which regulate microglial morphology and process dynamics (54, 55). Conceivably, knockout of NTPDase1 may cause microglial deramification by interrupting RanBPM signaling, independent of any changes in purinergic signaling. Further evidence for a lack of tonic ATP release and NTPDase1 activity under physiological conditions is the finding that extracellular adenosine levels are not generated by NTPDase-mediated ATP hydrolysis but mainly result from a direct release of adenosine from cells (56).

A key outcome of our study is that, surprisingly, all apyrase preparations that we tested, which are commonly used by researchers, were contaminated by a high $[K^+]$ content, which presumably arises from the process by which the apyrase is manufactured. Sigma-Aldrich is by far the most popular supplier of apyrase preparations for scientists. A Google Scholar search using the search terms "apyrase Axxxx" revealed the following numbers of publications for different Sigma-Aldrich apyrase types: A6132, 68; A6535, 97; A7646, 33; and A6410, 58 (though most publications list only the supplier's name without the catalog number). In experiments performed on brain slices and in vivo, apyrase is commonly used at concentrations of 100 to 300 U/mL (500 U/mL is the maximum), which corresponds to a rise of extracellular $[K^+]$ in the range of 5 to >80 mM.

Apyrase is commonly used in neurobiological studies due to the widespread role of ATP as a neurotransmitter (57). Using the search term "apyrase neuron" in National Center for Biotechnology Information/PubMed results in 111 publications, whereas "apyrase glia" gives 83 hits, of which the majority studied astrocytes (57 papers) and microglia (27 papers). For instance, in the astrocyte field, apyrase has been used in brain slices, retinal explants (ex vivo), or in vivo at higher doses between 25 and 300 U/mL to investigate the ATP dependence of astroglial calcium signaling (58, 59), mechanisms of ATP release from astrocytes (60–62), or astrocyte–neuron communication (63–65). Similarly for microglia, apyrase-induced depletion of extracellular purines in brain slices or in vivo has been used to investigate the role of extracellular ATP in (*i*) microglial baseline surveillance and targeted motility to focal tissue damage or an ATP source (3, 15–17, 25, 61, 66–68), (*ii*) microglia–astrocyte communication (3, 59, 69), (*iii*) ischemia-induced microglial death (70), and (*iv*) hypotonia-evoked microglial ATP release (71). Without questioning the conclusions of these studies, which usually reflect evidence from a number of different experimental approaches, the fact that undialyzed apyrase can strongly depolarize cells due to its accompanying $[K^+]$ content makes it essential to reassess some of the results obtained, particularly from experiments using a higher dose of apyrase. Protein dialysis provides a simple and effective way to remove the unwanted K^+

from apyrase while retaining its enzymatic activity, and we strongly advocate this procedure for any further studies using apyrase.

In conclusion, our study demonstrates that the extracellular ATP concentration in healthy brain tissue is not sufficient to drive tonic purinergic signaling in microglia, which is hence not required to maintain their surveillance and ramification under nonactivated "resting" conditions.

Materials and Methods

Brain Slice Preparation. Animal procedures were carried out in accordance with the guidelines of the UK Animals (Scientific Procedures) Act 1986 and subsequent amendments and were approved by the local Animal Welfare and Ethical Board. Acute hippocampal slices (300 μm thick; see schematic in Fig. 1*K*) were prepared (72) from P12 Sprague–Dawley rats of either sex, in ice-cold solution containing 124 mM NaCl, 26 mM $NaHCO_3$, 1 mM NaH_2PO_4, 2.5 mM KCl, 2 mM $MgCl_2$, 2 mM $CaCl_2$, 10 mM glucose, bubbled with 95% O_2/5% CO_2 (pH 7.4), as well as 1 mM Na-kynurenate to block glutamate receptors. Brain slicing does not activate microglia for at least 4 h, as judged by cell morphology, motility, and interleukin 1β release (73, 74), and allows pharmacological investigation of mechanisms in a manner that is not possible using in vivo experiments. Supporting this, surveillance and ramification of microglia were essentially constant during imaging for up to an hour in brain slices (figure 3D of ref. 33; Fig. 1 *G* and *H*) while in contrast the microglia would retract their processes and decrease surveillance if they were becoming activated. Slices were incubated for 30 min in darkness at room temperature (22 to 24 °C) in oxygenated Hepes-buffered external solution (see below) containing 25 μg/mL Alexa 594-conjugated isolectin B_4 (Thermo Fisher) for all experiments involving live imaging or 25 μg/mL Alexa 568-conjugated isolectin B_4 for electrophysiology experiments (73, 75), before being used in experiments. Isolectin B_4 labeling does not activate microglia (75), and its use avoids functional changes which might occur in transgenically labeled microglia.

Solutions and Electrophysiology. Slices were superfused with Hepes-buffered solution, at 34 to 36 °C for all experiments involving imaging and at room temperature (22 to 24 °C) for electrophysiology experiments, containing 140 mM NaCl, 2.5 mM KCl, 10 mM Hepes, 1 mM NaH_2PO_4, 2 mM $CaCl_2$, 1 mM $MgCl_2$, 10 mM glucose, pH set to 7.4 with NaOH, bubbled with 100% O_2. When the [KCl] was raised by 20 mM, [NaCl] was lowered by 20 mM. Cells were whole cell-clamped with electrodes containing KCl-based solution, comprising 125 mM KCl (or CsCl), 4 mM NaCl, 1 mM $CaCl_2$, 10 mM Hepes, 10 mM EGTA, 4 mM MgATP, 0.5 mM Na_2GTP, pH set to 7.1 with KOH or CsOH. The final osmolarity was 285 ± 5 mOsmol/kg. Microglia were identified by their fluorescent label and ramified morphology, and whole cell-clamped at a depth of ∼50 to 100 μm in the slice using borosilicate pipettes with a tip resistance of ∼4 to 5 MΩ, giving a series resistance of <20 MΩ. Electrode junction potentials were compensated. Current–voltage relations were from responses to 200-ms voltage steps ranging from −120 to +60 mV in 30-mV increments. Voltage- and current-clamp recordings were performed using a MultiClamp 700B amplifier (Molecular Devices). Currents were filtered at 1 kHz, digitized (10 kHz), and analyzed off-line using pClamp10 software.

Drugs and Dialysis. Drugs were obtained from Sigma-Aldrich or Tocris, and in live-imaging or electrophysiology experiments were applied via bath perfusion (ARL-67156; $BaCl_2$) or locally via pressure ejection from a puffing pipette placed at the slice surface (in the case of ATP). Apyrase was applied either directly as a bolus to the perfusion chamber with the flow temporarily stopped (in electrophysiology experiments) or added to a patch pipette inserted into the slice tissue and puffed onto an individual microglial cell that was real time-imaged (Fig. 1 *F–J*).

Dialysis of apyrase was performed using a 3-mL dialysis cassette (Slide-A-Lyzer, 2-kDa MWCO; Thermo Scientific; 87718) placed in cold dialysis buffer (Hepes-buffered extracellular solution) with 300× the sample volume for 2 h at 4 °C. The dialysis buffer was stirred and changed after 1 h.

Chemiluminescence Assay. ATP was measured with a luciferin/luciferase-based chemiluminescence assay which is specific for the detection of ATP. Superfusion of brain slices was halted and aliquots containing 25 μL of luciferin stock (Sigma; L9506; 12 mg/mL in extracellular solution) and 25 μL of luciferase stock (AppliChem; A1006; 6 mg/mL in 0.5 M Tris buffer, pH 7.5) were added to a total bath chamber volume of ∼0.5 mL at room temperature (as luciferase is not stable at higher temperatures). ATP-derived bioluminescence was detected using a photomultiplier tube (Thorn EMI Electronics; 9224B; input voltage set to 1,000 V) in darkness. This system is able to detect 6.2×10^{-11} M ATP (29). Photoelectrical currents were amplified, digitized, and recorded using pClamp10.

Potassium Measurements. Measurements of $[K^+]_e$ in experiments on brain slices were performed using custom-made potassium-sensitive electrodes fabricated and calibrated as described (76).

The $[K^+]$ in extracellular solution (without a slice) to which different apyrase preparations were added (at 100 U/mL) was also measured using a blood-gas analyzer (Siemens; RAPIDLab 348EX) set to dialysis mode. The inbuilt potassium sensor was calibrated according to the manufacturer's instructions, and measurements were interleaved with control extracellular solution containing a preset potassium concentration. Values in Fig. 3*F* refer to the total $[K^+]$ including the 2.5 mM KCl of the standard extracellular solution.

Two-Photon Imaging. Microglia in hippocampal slices were imaged at 34 to 36 °C, at a depth of ∼50 to 100 μm in the slice (to avoid studying superficial microglia that had started to become activated by the slicing procedure) using a Zeiss LSM 710 microscope (with a 20× lens, N.A. 1.0) and a Spectra-Physics Mai Tai DeepSee eHP Ti:sapphire infrared laser. For imaging of microglia labeled with isolectin B_4–Alexa 594, the laser was tuned to a wavelength of 800 nm; generally, the laser was adjusted to 1.8 to 2% of its maximum power, corresponding to ∼5 mW at the preparation. The pixel dwell time was 1 μs. For imaging of microglial surveillance, stacks of 21 to 31 slices imaged at 2-μm-depth intervals were acquired every 60 s. Images were typically 512 by 512 pixels and covered a square field of view 200 to 250 μm wide.

Image Analysis. Analysis of two-photon images was performed using custom-written ImageJ (NIH) and MATLAB scripts (The MathWorks), available at https://github.com/AttwellLab/Microglia. For analysis and quantification of microglial surveillance, each slice of every stack was filtered with a median filter after subtraction of smooth continuous background with the ImageJ "subtract background" plugin with a ball size of 30 pixels. The 4D stacks were then registered first for lateral drift, then rotated 90° on their side, registered for *z* drift, and rotated back to their original orientation. We then performed a maximum-intensity projection. Cells of interest were individually selected by manually drawing a region of interest (ROI) around an area including all their process extensions over the whole duration of the resulting 2D movie, and erasing data around that ROI. These 2D movies of individual cells were then manually binarized and saved as independent files.

To quantify surveillance, for each movie, starting with the second frame, we subtracted from each binarized frame F_t the preceding frame F_{t-1} and created two binarized movies, *PE* consisting of only the pixels containing process extensions ($F_t - F_{t-1} > 0$) and *PR* consisting of only the pixels containing process retractions ($F_t - F_{t-1} < 0$). In both *PE* and *PR*, all other pixels are set to 0. The baseline surveillance index *B* is defined as the sum over all nonzero pixels in *PE* + *PR* normalized by its average over the initial 20 min of each experiment, namely

$$B = \left(\sum_{\text{pixels}} PE + PR\right) \Big/ \left\langle \left(\sum_{\text{pixels}} PE + PR\right) \right\rangle_{\text{control}},$$

where Σ_{pixels} denotes a sum taken over all nonzero pixels and $\langle\ \rangle_{\text{control}}$ denotes a temporal average taken over the control period of the experiment (the first 20 min here). Surveillance indices were calculated as absolute values according to $B = (\Sigma_{\text{pixels}}\ PE + PR)$, and subsequently normalized to the control condition. The surveillance index provides a measure of the brain volume that is surveyed by a microglial cell in a given time. It is affected both by the rate at which processes elongate and shorten, and by the overall number of the microglial processes and their length.

To quantify ramification, in each movie frame, the MATLAB functions "bwarea" (uk.mathworks.com/help/images/ref/bwarea.html) and "bwperim" with eight-connected neighborhood (uk.mathworks.com/help/images/ref/bwperim.html) were used to quantify, respectively, the area and perimeter of the cell. The ramification index *R* is defined as the ratio of the perimeter to the area, normalized by that same ratio calculated for a circle of the same area. Specifically,

$$R = (\text{perimeter}/\text{area}) \Big/ \left[2 \times (\pi/\text{area})^{1/2}\right].$$

Thus, $R = 1$ if the cell is a perfect circle. The more ramified the cell, the larger *R* is. In 134 cells in hippocampal slices the mean value of *R* was 6.44 ± 0.14 at the beginning of the experiment.

Sholl Analysis. Microglial morphology was also assessed by Sholl analysis (77). Rat hippocampal brain slices were prepared as described above. After a 30-min recovery, slices were incubated at room temperature in oxygenated extracellular solution containing 100 or 200 U/mL apyrase (A7646) or 22.5 mM $[K^+]_e$ for 30 min (for Figs. 1 *A–E* and 3 *J–L*) or for 7.5 and 15 min (for Fig. 3*M*) followed by a further 15 min in solution without added apyrase or 22.5 mM $[K^+]_e$ to observe recovery from the effects of apyrase and K^+. Tissue sections were then fixed in 4% paraformaldehyde for 45 min. After washing three times for 15 min in PBS, slices were blocked and permeabilized in 10% normal goat serum and 0.25% Triton X-100 in PBS for 4 h at room temperature and then incubated at 4 °C overnight in rabbit anti–Iba-1 (234003; Synaptic Systems; 1:500) antibody prepared in blocking solution. After washing three times for 20 min in PBS, slices were incubated overnight in secondary antibody (goat anti-rabbit Alexa 543; Invitrogen; 1:500). Slices were then washed in PBS, incubated in DAPI (Invitrogen), and mounted on glass slides using Dako Fluorescence Mounting Medium. Z stacks of individual microglial cells located ∼60 μm below the slice surface were acquired at 0.3-μm-depth intervals using a 63× oil immersion objective (N.A. 1.4) on a Zeiss LSM 700 confocal microscope. Image stacks were preprocessed in ImageJ by median filtering ("despeckling") after subtraction of smooth continuous background with a ball size of 30 pixels and saved as TIF files. Reconstructions of individual microglial cells were carried out using 3D automatic cell tracing in Vaa3D software (www.vaa3d.org). Morphological parameters were then extracted using custom code written in MATLAB. The software used is available at https://github.com/AttwellLab/Microglia.

Statistics. Data are presented as mean ± SEM. *P* values are from two-tailed Student's *t* tests (for normally distributed data) or Mann–Whitney *U* tests (for nonnormally distributed data). Normality of data was checked using the Kolmogorov–Smirnov or Shapiro–Wilk test, and equality of variance was confirmed using the *F* test. Sholl analysis distributions were compared with a Kolmogorov–Smirnov test. For multiple comparisons, *P* values were corrected using a procedure equivalent to the Holm–Bonferroni method (for *N* comparisons, the most significant *P* value is multiplied by *N*, the second most significant by $N - 1$, the third most significant by $N - 2$, etc.; corrected *P* values are significant if they are less than 0.05).

ACKNOWLEDGMENTS. We thank Renaud Jolivet for discussion and software. This work was supported by the Wellcome Trust (099222/Z/12/Z) and European Research Council (BrainEnergy).

1. Madry C, Attwell D (2015) Receptors, ion channels, and signaling mechanisms underlying microglial dynamics. *J Biol Chem* 290:12443–12450.
2. Nimmerjahn A, Kirchhoff F, Helmchen F (2005) Resting microglial cells are highly dynamic surveillants of brain parenchyma in vivo. *Science* 308:1314–1318.
3. Davalos D, et al. (2005) ATP mediates rapid microglial response to local brain injury in vivo. *Nat Neurosci* 8:752–758.
4. Honda S, et al. (2001) Extracellular ATP or ADP induce chemotaxis of cultured microglia through $G_{i/o}$-coupled P2Y receptors. *J Neurosci* 21:1975–1982.
5. Haynes SE, et al. (2006) The $P2Y_{12}$ receptor regulates microglial activation by extracellular nucleotides. *Nat Neurosci* 9:1512–1519.
6. Prinz M, Priller J (2014) Microglia and brain macrophages in the molecular age: From origin to neuropsychiatric disease. *Nat Rev Neurosci* 15:300–312.
7. Wolf SA, Boddeke HWGM, Kettenmann H (2017) Microglia in physiology and disease. *Annu Rev Physiol* 79:619–643.
8. Wake H, Moorhouse AJ, Jinno S, Kohsaka S, Nabekura J (2009) Resting microglia directly monitor the functional state of synapses in vivo and determine the fate of ischemic terminals. *J Neurosci* 29:3974–3980.
9. Tremblay M-È, Lowery RL, Majewska AK (2010) Microglial interactions with synapses are modulated by visual experience. *PLoS Biol* 8:e1000527.
10. Li Y, Du XF, Liu CS, Wen ZL, Du JL (2012) Reciprocal regulation between resting microglial dynamics and neuronal activity in vivo. *Dev Cell* 23:1189–1202.
11. Paolicelli RC, et al. (2011) Synaptic pruning by microglia is necessary for normal brain development. *Science* 333:1456–1458.
12. Schafer DP, et al. (2012) Microglia sculpt postnatal neural circuits in an activity and complement-dependent manner. *Neuron* 74:691–705.
13. Marín-Teva JL, et al. (2004) Microglia promote the death of developing Purkinje cells. *Neuron* 41:535–547.
14. Sierra A, et al. (2010) Microglia shape adult hippocampal neurogenesis through apoptosis-coupled phagocytosis. *Cell Stem Cell* 7:483–495.
15. Kurpius D, Nolley EP, Dailey ME (2007) Purines induce directed migration and rapid homing of microglia to injured pyramidal neurons in developing hippocampus. *Glia* 55:873–884.
16. Fontainhas AM, et al. (2011) Microglial morphology and dynamic behavior is regulated by ionotropic glutamatergic and GABAergic neurotransmission. *PLoS One* 6: e15973.
17. Eyo U, Dailey ME (2012) Effects of oxygen-glucose deprivation on microglial mobility and viability in developing mouse hippocampal tissues. *Glia* 60:1747–1760.
18. Braun N, et al. (2000) Assignment of ecto-nucleoside triphosphate diphosphohydrolase-1/cd39 expression to microglia and vasculature of the brain. *Eur J Neurosci* 12: 4357–4366.
19. Zimmermann H (2000) Extracellular metabolism of ATP and other nucleotides. *Naunyn Schmiedebergs Arch Pharmacol* 362:299–309.
20. Joseph SM, Buchakjian MR, Dubyak GR (2003) Colocalization of ATP release sites and ecto-ATPase activity at the extracellular surface of human astrocytes. *J Biol Chem* 278: 23331–23342.
21. Melani A, et al. (2005) ATP extracellular concentrations are increased in the rat striatum during in vivo ischemia. *Neurochem Int* 47:442–448.
22. Wall MJ, Atterbury A, Dale N (2007) Control of basal extracellular adenosine concentration in rat cerebellum. *J Physiol* 582:137–151.
23. Heinrich A, Andó RD, Túri G, Rózsa B, Sperlágh B (2012) K^+ depolarization evokes ATP, adenosine and glutamate release from glia in rat hippocampus: A microelectrode biosensor study. *Br J Pharmacol* 167:1003–1020.
24. Abbracchio MP, et al. (2006) International Union of Pharmacology LVIII: Update on the P2Y G protein-coupled nucleotide receptors: From molecular mechanisms and pathophysiology to therapy. *Pharmacol Rev* 58:281–341.
25. Sieger D, Moritz C, Ziegenhals T, Prykhozhij S, Peri F (2012) Long-range Ca^{2+} waves transmit brain-damage signals to microglia. *Dev Cell* 22:1138–1148.
26. Sipe GO, et al. (2016) Microglial $P2Y_{12}$ is necessary for synaptic plasticity in mouse visual cortex. *Nat Commun* 7:10905.
27. Handa M, Guidotti G (1996) Purification and cloning of a soluble ATP-diphosphohydrolase (apyrase) from potato tubers (*Solanum tuberosum*). *Biochem Biophys Res Commun* 218:916–923.
28. Seliger HH, McElroy WD (1960) Spectral emission and quantum yield of firefly bioluminescence. *Arch Biochem Biophys* 88:136–141.
29. Wieraszko A, Goldsmith G, Seyfried TN (1989) Stimulation-dependent release of adenosine triphosphate from hippocampal slices. *Brain Res* 485:244–250.
30. Zimmermann H, Zebisch M, Sträter N (2012) Cellular function and molecular structure of ecto-nucleotidases. *Purinergic Signal* 8:437–502.
31. Dunwiddie TV, Diao L, Proctor WR (1997) Adenine nucleotides undergo rapid, quantitative conversion to adenosine in the extracellular space in rat hippocampus. *J Neurosci* 17:7673–7682.
32. Wall MJ, Dale N (2007) Auto-inhibition of rat parallel fibre-Purkinje cell synapses by activity-dependent adenosine release. *J Physiol* 581:553–565.
33. Madry C, et al. (2017) Microglial ramification, surveillance and interleukin-1β release are regulated by the two-pore domain K^+ channel THIK-1. *Neuron*, 10.1016/j.neuron.2017.12.002.
34. Iqbal J, Vollmayer P, Braun N, Zimmermann H, Müller CE (2005) A capillary electrophoresis method for the characterization of ecto-nucleoside triphosphate diphosphohydrolases (NTPDases) and the analysis of inhibitors by in-capillary enzymatic microreaction. *Purinergic Signal* 1:349–358.
35. Lévesque SA, Lavoie ÉG, Lecka J, Bigonnesse F, Sévigny J (2007) Specificity of the ecto-ATPase inhibitor ARL 67156 on human and mouse ectonucleotidases. *Br J Pharmacol* 152:141–150.
36. Dissing-Olesen L, et al. (2014) Activation of neuronal NMDA receptors triggers transient ATP-mediated microglial process outgrowth. *J Neurosci* 34:10511–10527.
37. De Biase LM, et al. (2017) Local cues establish and maintain region-specific phenotypes of basal ganglia microglia. *Neuron* 95:341–356.e6.
38. Lauritzen M, et al. (2011) Clinical relevance of cortical spreading depression in neurological disorders: Migraine, malignant stroke, subarachnoid and intracranial hemorrhage, and traumatic brain injury. *J Cereb Blood Flow Metab* 31:17–35.
39. Hansen AJ (1985) Effect of anoxia on ion distribution in the brain. *Physiol Rev* 65: 101–148.
40. Zhang Y, et al. (2014) An RNA-sequencing transcriptome and splicing database of glia, neurons, and vascular cells of the cerebral cortex. *J Neurosci* 34:11929–11947.
41. Matyash M, Zabiegalov O, Wendt S, Matyash V, Kettenmann H (2017) The adenosine generating enzymes CD39/CD73 control microglial processes ramification in the mouse brain. *PLoS One* 12:e0175012.
42. Hamann M, Attwell D (1996) Non-synaptic release of ATP by electrical stimulation in slices of rat hippocampus, cerebellum and habenula. *Eur J Neurosci* 8:1510–1515.
43. Frenguelli BG, Wigmore G, Llaudet E, Dale N (2007) Temporal and mechanistic dissociation of ATP and adenosine release during ischaemia in the mammalian hippocampus. *J Neurochem* 101:1400–1413.
44. Färber K, et al. (2008) The ectonucleotidase cd39/ENTPDase1 modulates purinergic-mediated microglial migration. *Glia* 56:331–341.
45. Ohsawa K, et al. (2012) Adenosine A3 receptor is involved in ADP-induced microglial process extension and migration. *J Neurochem* 121:217–227.
46. Lanser AJ, et al. (2017) Disruption of the ATP/adenosine balance in $CD39^{-/-}$ mice is associated with handling-induced seizures. *Immunology* 152:589–601.
47. Sévigny J, et al. (2002) Differential catalytic properties and vascular topography of murine nucleoside triphosphate diphosphohydrolase 1 (NTPDase1) and NTPDase2 have implications for thromboregulation. *Blood* 99:2801–2809.
48. Robson SC, et al. (2005) Ectonucleotidases of CD39 family modulate vascular inflammation and thrombosis in transplantation. *Semin Thromb Hemost* 31:217–233.
49. Antonioli L, Pacher P, Vizi ES, Haskó G (2013) CD39 and CD73 in immunity and inflammation. *Trends Mol Med* 19:355–367.
50. Rymo SF, et al. (2011) A two-way communication between microglial cells and angiogenic sprouts regulates angiogenesis in aortic ring cultures. *PLoS One* 6:e15846.

51. Dudvarski Stankovic N, Teodorczyk M, Ploen R, Zipp F, Schmidt MHH (2016) Microglia-blood vessel interactions: A double-edged sword in brain pathologies. *Acta Neuropathol* 131:347–363.
52. Wu Y, et al. (2006) RanBPM associates with CD39 and modulates ecto-nucleotidase activity. *Biochem J* 396:23–30.
53. Woo JA, Roh S-E, Lakshmana MK, Kang DE (2012) Pivotal role of RanBP9 in integrin-dependent focal adhesion signaling and assembly. *FASEB J* 26:1672–1681.
54. Ohsawa K, et al. (2010) $P2Y_{12}$ receptor-mediated integrin-β1 activation regulates microglial process extension induced by ATP. *Glia* 58:790–801.
55. Kim C, et al. (2014) β1-Integrin-dependent migration of microglia in response to neuron-released α-synuclein. *Exp Mol Med* 46:e91.
56. Melani A, et al. (2012) Ecto-ATPase inhibition: ATP and adenosine release under physiological and ischemic in vivo conditions in the rat striatum. *Exp Neurol* 233: 193–204.
57. Burnstock G (2006) Historical review: ATP as a neurotransmitter. *Trends Pharmacol Sci* 27:166–176.
58. Newman EA (2005) Calcium increases in retinal glial cells evoked by light-induced neuronal activity. *J Neurosci* 25:5502–5510.
59. Kurth-Nelson ZL, Mishra A, Newman EA (2009) Spontaneous glial calcium waves in the retina develop over early adulthood. *J Neurosci* 29:11339–11346.
60. Gourine AV, et al. (2010) Astrocytes control breathing through pH-dependent release of ATP. *Science* 329:571–575.
61. Vázquez C, et al. (2015) Endocannabinoids regulate the activity of astrocytic hemichannels and the microglial response against an injury: In vivo studies. *Neurobiol Dis* 79:41–50.
62. Guthrie PB, et al. (1999) ATP released from astrocytes mediates glial calcium waves. *J Neurosci* 19:520–528.
63. Koizumi S, Fujishita K, Tsuda M, Shigemoto-Mogami Y, Inoue K (2003) Dynamic inhibition of excitatory synaptic transmission by astrocyte-derived ATP in hippocampal cultures. *Proc Natl Acad Sci USA* 100:11023–11028.
64. Koizumi S, Fujishita K, Inoue K (2005) Regulation of cell-to-cell communication mediated by astrocytic ATP in the CNS. *Purinergic Signal* 1:211–217.
65. Zhang X, Chen Y, Wang C, Huang L-YM (2007) Neuronal somatic ATP release triggers neuron-satellite glial cell communication in dorsal root ganglia. *Proc Natl Acad Sci USA* 104:9864–9869.
66. Dibaj P, et al. (2010) NO mediates microglial response to acute spinal cord injury under ATP control in vivo. *Glia* 58:1133–1144.
67. Dibaj P, et al. (2010) Long-lasting post-mortem activity of spinal microglia in situ in mice. *J Neurosci Res* 88:2431–2440.
68. Dou Y, et al. (2012) Microglial migration mediated by ATP-induced ATP release from lysosomes. *Cell Res* 22:1022–1033.
69. Kim JV, Dustin ML (2006) Innate response to focal necrotic injury inside the blood-brain barrier. *J Immunol* 177:5269–5277.
70. Eyo UB, Miner SA, Ahlers KE, Wu L-J, Dailey ME (2013) $P2X_7$ receptor activation regulates microglial cell death during oxygen-glucose deprivation. *Neuropharmacology* 73:311–319.
71. Murana E, et al. (2017) ATP release during cell swelling activates a Ca^{2+}-dependent Cl^- current by autocrine mechanism in mouse hippocampal microglia. *Sci Rep* 7:4184.
72. Bischofberger J, Engel D, Li L, Geiger JR, Jonas P (2006) Patch-clamp recording from mossy fiber terminals in hippocampal slices. *Nat Protoc* 1:2075–2081.
73. Kurpius D, Wilson N, Fuller L, Hoffman A, Dailey ME (2006) Early activation, motility, and homing of neonatal microglia to injured neurons does not require protein synthesis. *Glia* 54:58–70.
74. Gyoneva S, Traynelis SF (2013) Norepinephrine modulates the motility of resting and activated microglia via different adrenergic receptors. *J Biol Chem* 288:15291–15302.
75. Grinberg YY, Milton JG, Kraig RP (2011) Spreading depression sends microglia on Lévy flights. *PLoS One* 6:e19294.
76. Hamilton NB, Kolodziejczyk K, Kougioumtzidou E, Attwell D (2016) Proton-gated Ca^{2+}-permeable TRP channels damage myelin in conditions mimicking ischaemia. *Nature* 529:523–527.
77. Sholl DA (1953) Dendritic organization in the neurons of the visual and motor cortices of the cat. *J Anat* 87:387–406.
78. Wendt S, Wogram E, Korvers L, Kettenmann H (2016) Experimental cortical spreading depression induces NMDA receptor dependent potassium currents in microglia. *J Neurosci* 36:6165–6174.
79. Lopatin AN, Nichols CG (1996) $[K^+]$ dependence of polyamine-induced rectification in inward rectifier potassium channels (IRK1, Kir2.1). *J Gen Physiol* 108:105–113.